Article

Discovery Medicine 2026; 38(207): 1311–1326
https://doi.org/10.24976/Discov.Med.202638207.104

TRIM34 Accelerates Cardiac Fibrosis by Regulating the SMAD7 Transcription Through HNRNPL Ubiquitination

Yan Huang[1], Bingying Wang[1,*]

[1]Department of Clinical Laboratory, The Second Affiliated Hospital of Soochow University, 215000 Suzhou, Jiangsu, China
*Correspondence: bywang3059@163.com (Bingying Wang)
Submitted: 21 January 2026 Revised: 25 March 2026 Accepted: 31 March 2026 Published: 20 April 2026

Background: Cardiac fibrosis, characterized by aberrant cardiac fibroblast (CFs) activity and extracellular matrix deposition, is a fundamental pathological process underlying multiple heart diseases. Tripartite motif 34 (TRIM34), a K63-linked ubiquitin ligase, is upregulated in failing human hearts, yet its function in cardiac fibrosis remains unclear. This study aims to investigate the role of TRIM34 in cardiac fibrosis.

Methods: *In vivo*, fibrosis was induced by myocardial infarction (MI) via left anterior descending coronary artery ligation in mice, while TRIM34 knockdown was achieved using recombinant adenovirus-mediated shRNA. Fibrosis area and related markers were evaluated. *In vitro*, cardiac fibroblasts were treated with transforming growth factor beta 1 (TGF-β1) and transfected with shTRIM34; proliferation, migration, invasion, and fibroblast activation markers were assessed. Protein interaction, ubiquitination, and promoter activity were examined. Rescue experiments were performed using SMAD family member 7 (SMAD7) or heterogeneous nuclear ribonucleoprotein L (HNRNPL) knockdown.

Results: Upregulation of TRIM34 was found in fibrotic tissue of mice and TGF-β1-exposed CFs. Knockdown of TRIM34 reduced the cardiac fibrosis area and the expression of fibrosis markers in MI mice. Also, TRIM34 knockdown decreased the cell viability, numbers of migrated and invaded cells, and the level of myofibroblast marker, with the increased level of fibroblast markers in TGF-β1-induced CFs. Moreover, TRIM34 directly interacted and promoted ubiquitination degradation of HNRNPL. Furthermore, TRIM34 suppressed the transcription of the SMAD7 promoter by inhibiting the expression of HNRNPL. Rescue experiments showed that knockdown of HNRNPL or SMAD7 counteracted the antifibrotic role of shTRIM34 in MI mice and TGF-β1-exposed CFs.

Conclusion: TRIM34 exacerbated cardiac fibrosis by ubiquitinating HNRNPL and regulating SMAD7 expression, highlighting TRIM34 as a potential therapeutic target for fibrotic heart disease.

Keywords: myocardial fibrosis; myocardial infarction; TRIM34; ubiquitination; HNRNPL; SMAD7

Introduction

Cardiac fibrosis, characterized by preternatural proliferation of cardiac fibroblasts (CFs) and extracellular matrix (ECM) deposition, is a central pathological process driving heart failure [1,2]. Resident CFs activate and differentiate into myofibroblasts during ischemic injuries, such as the myocardial infarction (MI) [3,4]. Active myofibroblasts move and aggregate in injured regions of myocardium, and extend the border areas in most cardiac pathologic states, generating collagens and other ECM [5]. Eventually, cardiac fibrosis induces pathological alterations that lead to chamber dilatation, left ventricular strain, cardiomyocyte hypertrophy and cell apoptosis, thereby contributing to the progression of heart failure (HF) [6,7]. Despite its significance, therapeutic strategies directly targeting fibrotic pathways remain limited, highlighting the need to identify novel regulatory molecules.

Members of the tripartite motif (TRIM) family, many of which possess E3 ubiquitin ligase activity, are increasingly recognized as critical regulators of cellular signaling and disease progression [8–11]. Tripartite motif 34 (TRIM34), a less-studied member of the TRIM family, has been shown to interact with TRIM5α in primates, functioning together as a broadly-conserved lentiviral restriction factor [12]. More importantly, our preliminary experiments suggested that the expression of TRIM34 was increased in the heart tissue from patients with end-stage heart failure based on the GSE84796 microarray dataset. However, its role in cardiac fibrosis is entirely unknown. Therefore, we hypothesized that TRIM34 might function as a pro-fibrotic regulator.

To explore the mechanism, we focused on the known anti-fibrotic axis involving heterogeneous nuclear ribonucleoprotein L (HNRNPL) and SMAD family member 7 (SMAD7). HNRNPL promotes the transcription of

SMAD7, a potent endogenous inhibitor of the pro-fibrotic TGF-β/SMAD pathway, thereby suppressing myofibroblast activation and fibrosis [13,14]. Notably, HNRNPL stability is regulated by ubiquitin-mediated proteasomal degradation [15]. We therefore speculated that TRIM34 might exacerbate cardiac fibrosis by acting as an E3 ligase to ubiquitinate and degrade HNRNPL, leading to downregulation of SMAD7.

This study, to the best of our knowledge, is the first report of TRIM34 in myocardial fibrosis, and aims to investigate the role of TRIM34 in cardiac fibrosis and to test this TRIM34/HNRNPL/SMAD7 regulatory axis using *in vivo* myocardial infarction models and *in vitro* CFs models. The outcomes revealed that TRIM34 exacerbated cardiac fibrosis by ubiquitinating HNRNPL and regulating SMAD7 expression, highlighting TRIM34 as a potential therapeutic target for fibrotic heart disease.

Materials and Methods

TRIM34 Expression In Silico

The GSE84796 microarray dataset was extracted from the Agilent-028004 SurePrint G3 Human GE 8x60K Microarray platform according to the GEO database. The dataset comprised seven control samples from the left ventricular free wall of healthy donor hearts, and ten patient samples from the left ventricular free wall of patients with end-stage heart failure. The TRIM34 expression was analyzed in control and ischemic cardiomyopathy groups using the LIMMA package in R language.

Animals

Healthy C57BL/6 mice (8-week-old, 20 $\pm$ 2 g) were bought from Cyagen (Suzhou, China) and raised in a temperature-controlled laboratory with a 12-h cycle of light-dark, as well as rodent chow and water *ad libitum*. Animal experiments were conducted in compliance with the Guide for the Care and Use of Laboratory Animals [16] and approved by the Animal Research Ethics Committee of the Second Affiliated Hospital of Soochow University (Approval No. EC2022(131)).

Induction of MI in Mice

MI was induced in mice as previously described [17]. Mice were anesthetized through isoflurane (catalog number: R510-22, RWD, Shenzhen, China) and ventilated with a small animal ventilator (catalog number: R500, RWD). Mice were subjected to the left-sided thoracotomy through the fourth intercostal space, and the heart was exposed by opening the pericardium. A 7/0 nylon suture was used to ligate the left descending coronary artery (LAD) at 2 mm under the border between the left atrium and ventricle to evoke MI. A prominent S-T segment elevation recorded by an electrocardiograph indicated myocardial ischemia. The sham mice experienced the same experimental procedures as the MI mice without ligation of LAD. After the operation, mice were monitored every day for their health and activity state as well as signs of infection. Mice were sacrificed at four weeks following MI.

Animal Management

After excluding mice that died from surgery or had failed ligation, the remaining mice were randomly assigned to each group. To systematically investigate the role and mechanism of TRIM34 *in vivo*, the study was structured into eight sequential experimental phases.

The first, second and third experimental phases were to assess the establishment of the MI model and the examination of TRIM34 expression. In these three experimental phases, mice were randomly assigned to two groups (n = 6 per group): a sham group and an MI group. In the first experimental phase, 12 mice were randomly assigned to two groups, and their hearts were stained with 2,3,5-triphenyltetrazolium chloride (TTC). In the second experimental phase, 12 mice were randomly assigned to two groups, and their hearts were stained pathologically and subjected to immunofluorescence (IF) assays. In the third experimental phase, 12 mice were randomly assigned to two groups, and their hearts were used for quantitative RT-PCR (RT-qPCR) and Western blot analyses.

The fourth, fifth and sixth experimental phases were to assess the influence of TRIM34 knockdown. Mice were randomly assigned to four groups (n = 6 per group): a sham+Ad-shNC group, a sham+Ad-shTRIM34 group, an MI+Ad-shNC group, and an MI+Ad-shTRIM34 group. In the fourth experimental phase, 24 mice were randomly assigned to four groups, and their hearts were stained with TTC. In the fifth experimental phase, 24 mice were randomly assigned to four groups, and their hearts were stained pathologically. In the sixth experimental phase, 24 mice were randomly assigned to four groups, and their hearts were used for Western blot analysis.

The seventh and eighth experimental phases were the rescue experiments to verify the specificity of the TRIM34/HNRNPL/SMAD7 axis. Mice were randomly assigned to five groups (n = 6 per group): sham, MI+Ad-shNC, MI+Ad-shTRIM34, MI+Ad-shTRIM34+Ad-shSMAD7 and MI+Ad-shTRIM34+Ad-shHNRNPL. In the seventh experimental phase, 30 mice were randomly assigned to five groups, and their hearts were stained pathologically. In the eighth experimental phase, 30 mice were randomly assigned to five groups, and their hearts were used for Western blot analysis.

MI mice were induced by permanent ligation of the LAD, while sham mice underwent the same procedure without LAD ligation. To inhibit the expression of TRIM34 and SMAD7, short hairpin RNA (shRNA) targeting TRIM34, SMAD7 and HNRNPL were synthesized and packaged into recombinant adenovirus by Genechem (Shanghai, China). All shRNA sequences used in this study

were as follows: shTRIM34: 5′-CACCGGAGGAACTTATCTCGGATCTCGAAAGATCCGAGATAAGTTCCTCC-3′, shSMAD7: 5′-CACCGCACTCGGTGCTCAAGAAACTCGAAAGTTTCTTGAGCACCGAGTGC-3′, shHNRNPL: 5′-CCGGACGCAAAGCCTACGCGTTTAACTCGAGTTAAACGCGTAGGCTTTGCGTTTTTTG-3′, and shNC: 5′-CCGGCAACAAGATGAAGAGCACCAACTCGAGTTGGTGCTCTTCATCTTGTTGTTTTTG-3′. The virus was administered at a dose of 3×10^{11} viral particles (vp) per mouse in a total volume of 80 µL sterile phosphate-buffered saline (PBS) based on the previous study [18] and our preliminary results. Mice underwent a single intramyocardial injection of adenovirus packaged with shTRIM34 (Ad-shTRIM34), shSMAD7 (Ad-shSMAD7), and a negative control of shRNA (Ad-shNC) for two weeks before the MI operation.

Thus, mice in the MI+Ad-shTRIM34+Ad-shSMAD7 group were intramyocardially injected with 3×10^{11} vp Ad-shTRIM34 and Ad-shSMAD7 per mouse for two weeks, and then induced with MI. Mice in the MI+Ad-shTRIM34+Ad-shHNRNPL group were intramyocardially injected with 3×10^{11} vp Ad-shTRIM34 and Ad-shHNRNPL per mouse for two weeks, and then induced with MI. Mice in the MI+Ad-shTRIM34 group were intramyocardially injected with 3×10^{11} vp Ad-shTRIM34 per mouse for two weeks, and then induced with MI. Mice in the MI+Ad-shNC group were intramyocardially injected with 3×10^{11} vp Ad-shNC per mouse for two weeks, and then induced with MI. Mice in the sham+Ad-shTRIM34 group were intramyocardially injected with 3×10^{11} vp Ad-shTRIM34 per mouse for two weeks, and then treated with the same procedures in the sham group as described above. Mice in the sham+Ad-shNC group were intramyocardially injected with 3×10^{11} vp Ad-shNC per mouse for two weeks, and then treated with the same procedures in the sham group as described above. Mice in the MI group were induced with MI as described above. Mice in the sham group were managed with the same procedures in the sham group as described above. Four weeks after MI, mice were sacrificed by inhaling excess isoflurane, and the heart tissues were harvested for subsequent detection.

TTC Staining

Hearts were rapidly dissected and sectioned coronally (2-mm intervals). Slices were stained with 1% TTC (catalog number: G3005, Solarbio, Beijing, China) at 37 °C for 20 min. Infarct areas were quantified using Image-Pro Plus 6.0, calculated as: (infarct volume / total contralateral volume) × 100%. Sections were mounted with neutral resin (catalog number: G8590, Solarbio) and imaged using a camera (Nikon, Japan).

Pathological Staining

The heart tissues were removed from mice and immersed in 4% paraformaldehyde (catalog number: P1110, Solarbio), and underwent dehydration and embedding. 5 µm-thickness slices were dyed with hematoxylin-eosin (HE) (catalog number: G1120, Solarbio) and Masson's Trichrome Stain Kit (catalog number: G1340, Solarbio). Slices were mounted with neutral resin (catalog number: G8590, Solarbio) and imaged using a digital trinocular camera microscope (lot number: CX23, Olympus, Tokyo, Japan). The percentage of cardiac fibrosis area was quantified through the measurement of collagen deposition (blue) on Masson's trichrome-dyed regions using Image-Pro Plus 6.0 (Media Cybernetics, Rockville, MD, USA).

Detection of the Level of Creatine Kinase Myocardial Band (CK-MB) and Troponin I (cTnI) in Sera

The serum levels of creatine kinase myocardial band (CK-MB) and cTnI were examined with the creatine kinase MB isoenzyme assay kit (catalog number: H197-1-1) and the troponin I (cTnI) assay kit (catalog number: E019, both from Nanjing Jiancheng Bioengineering Institute, Nanjing, China) according to the manufacturer's instructions. Briefly, for each assay, serum samples were appropriately diluted (CK-MB: 1:10; cTnI: 1:5). Standards and diluted samples (100 µL per well) were added to the antibody-precoated 96-well microplates and incubated at 37 °C for 60 minutes. After washing four times with the provided wash buffer, 100 µL of horseradish peroxidase (HRP)-conjugated detection antibody was added to each well and incubated at 37 °C for an additional 60 minutes. Following another washing step, 90 µL of chromogenic substrate (TMB) was added and incubated for 15–20 minutes at room temperature in the dark. The enzymatic reaction was stopped by adding 50 µL of stop solution, and the absorbance was immediately measured at 450 nm (for CK-MB) or 600 nm (for cTnI) using a microplate reader.

Cell Treatment

Mouse CFs were bought from Procell (catalog number: CP-M074, Wuhan, China) and grown in Mouse Cardiac Fibroblast Complete Medium (catalog number: CM-M074, Procell) for 24 h at 37 °C with 5% CO_2. Mycoplasma contamination in the cells was examined using a mycoplasma polymerase chain reaction (PCR) detection kit (catalog number: C0301S, Beyotime, Shanghai, China), and the tests were negative. Mouse cardiac fibroblasts were identified as adherent, spindle-shaped cells with a central oval nucleus and multiple cytoplasmic extensions, showing no rhythmic contraction. CFs were exposed to 20 ng/mL transforming growth factor beta 1 (TGF-β1) (catalog number: ab50036, Abcam, Cambridge, UK) for 24 h [17], and then subjected to the following assays. To downregulate the expression of TRIM34, HNRNPL and SMAD7 in CFs, shTRIM34, shHNRNPL, shSMAD7 and the homologous shNC provided by Genechem were transfected into CFs. The transfection was conducted using Lipofectamine 3000 (catalog number: L3000001, Invitrogen, Carlsbad, CA,

USA). Briefly, for each well of a 6-well plate, 2.5 µg of shRNA or shNC was diluted in 125 µL of Opti-MEM reduced serum medium. Separately, 5 µL of Lipofectamine 3000 reagent was diluted in 125 µL of Opti-MEM. The diluted shRNA or shNC was then combined with the diluted Lipofectamine 3000 reagent (1:1 ratio), mixed gently, and incubated at room temperature for 15 minutes to allow complex formation. The shRNA or shNC-lipid complexes were added dropwise to the cells in complete growth medium. The medium was replaced with fresh complete medium 6 hours post-transfection. Cells were harvested for subsequent assays 48 hours after transfection.

Cell Counting Kit-8 (CCK-8) Assays

CFs were inoculated in 96-well plates with a density of 1×10^5/well and grown with 5% CO_2 at 37 °C. Cell viability was assessed using the CCK-8 kit (catalog number: CA1210, Solarbio). The absorbance was read at 450 nm using a microplate reader (Thermo Fisher Scientific, Waltham, MA, USA).

Transwell Assays

For the invasion assays, CFs were seeded into the upper chamber of Transwell plates (catalog number: 3422, Corning Company, New York, NY, USA) coated with Matrigel (catalog number: 356234, Solarbio) and cultured in DMEM without FBS. After 24 h, the Matrigel was abrased, and the cells were immobilized with 4% paraformaldehyde (catalog number: P1110, Solarbio), dyed with 0.1% crystal violet (catalog number: G1063, Solarbio), and imaged under a microscope (Olympus). The migration assays were conducted in the same manner as the invasion assays without Matrigel. Numbers of invasive and migratory cells were enumerated by selecting five different and random fields to assess the cell invasion and migration ability.

Co-immunoprecipitation (Co-IP) Assay

CFs underwent lysis using cell disruption solution (catalog number: R0100, Solarbio) containing protease inhibitor cocktail (catalog number: A8260, Solarbio) at 0–4 °C for 40 minutes to collect the soluble fraction. For protein interaction analysis between TRIM34 and HNRNPL, primary antibodies against TRIM34 (catalog number: bs-9244R, Bioss, Beijing, China), HNRNPL (catalog number: ab264340, Abcam), or control IgG (catalog number: ab172730, Abcam) were incubated with lysates at 4 °C for 12 hours. Protein A/G magnetic beads (catalog number: 78609, Thermo Fisher Scientific) were subsequently supplemented with the mixtures and maintained under gentle agitation at 4 °C. Following magnetic separation, cell pellets were collected and washed three times with chilled lysis buffer. The immunocomplexes were denatured in electrophoresis sample buffer (catalog number: P1040, Solarbio) at 95 °C for 5 minutes before being subjected to immunoblotting analysis.

Ubiquitination Assay

Cellular lysates from CFs underwent immunoprecipitation with HNRNPL-specific antibodies, followed by immunoblotting with a K63-linked ubiquitin detection reagent (catalog number: 5621, Cell Signaling Technology Inc., Danvers, MA, USA). The precipitated complexes were subsequently resolubilized in SDS-containing lysis buffer (catalog number: S8010, Solarbio 1% concentration), thermally denatured for 10 minutes, and centrifuged at 12,000 g for 1 minute to obtain clarified supernatants. These supernatants were then analyzed through immunoblotting employing antibodies targeting both TRIM34 and HNRNPL.

Cycloheximide Assay

For protein stability assessment, CFs with TRIM34 knockdown (shTRIM34) or control cells (shNC) received cycloheximide treatment (catalog number: 239763-M, Sigma-Aldrich, St. Louis, MO, USA, 100 µg/mL) to inhibit new protein synthesis based on our previous study [19]. Cells were harvested at specified intervals (0, 1, 3, 6 hours post-treatment) and lysed using RIPA buffer (catalog number: R0010, Solarbio) supplemented with protease inhibitors for subsequent immunoblotting analysis.

Luciferase Reporter Assays

To investigate the regulatory function of TRIM34 in SMAD7 transcriptional activation, dual-luciferase reporter gene analysis was performed using progressive truncations of the SMAD7 promoter. The SMAD7 promoter region spanning from –2000 to +200 bp was inserted into the pGL3-Basic luciferase reporter plasmid (2 µg/mL, catalog number: E1751, Promega, Madison, WI, USA; the sequences were shown in https://www.promega.com/products/luciferase-assays/genetic-reporter-vectors-and-cell-lines/pgl3-luciferase-reporter-vectors/~/media/7D655F96608E4E06BB65844C7AF9F4C2.ashx) and subsequently co-transfected with TRIM34 expression vectors into CFs. After 48-hour culture in DMEM medium, enzymatic activity were measured using the assay kit (catalog number: E1910, Promega), with firefly luciferase signals normalized to Renilla luciferase controls for quantitative analysis.

Chromatin Immunoprecipitation (ChIP)

The chromatin immunoprecipitation (ChIP) assay was conducted to investigate the DNA fragments interacting with TRIM34 and SMAD7, as well as HNRNPL and SMAD7, utilizing the EZ-Magna ChIP A/G kit (catalog number: 17-371, Millipore, Billerica, MA, USA). CFs were crosslinked using 4% paraformaldehyde under ambient conditions for 10 minutes. Subsequent treatment with cell lysis buffer followed by nuclear lysis buffer facilitated chromatin isolation. Chromatin fragments were then sonicated to generate DNA segments of 500–800 base

Table 1. The sequences of primers used in the present study.

Gene	Forward sequence (5′-3′)	Reversed sequence (5′-3′)
TRIM34	CAACCATGGATCACTCATTTACAAG	CCCAAGGATTGAAGTATGGATAGG
SMAD7	CCTGCCATTGTAGCGTCTTTC	CCCTTGGGAAGCCCATCT
β-actin	CAGCCTTCCTTCTTGGGTATG	GGCATAGAGGTCTTTACGGATG

TRIM34, Tripartite motif 34; SMAD7, SMAD family member 7.

pairs, and then incubated with specific antibodies against TRIM34 (catalog number: bs-9244R, Bioss), HNRNPL (catalog number: ab264340, Abcam), or control IgG antibodies. Antibody-bound complexes were captured through overnight incubation at 4 °C with protein A/G-conjugated magnetic beads. Immunoprecipitated DNA was subsequently eluted, purified, and quantified through quantitative real-time PCR analysis.

RT-qPCR

Cardiac tissue and CF-derived RNA samples were isolated using TRIzol reagent (catalog number: 15596026, Thermo Fisher Scientific) followed by reverse transcription into complementary DNA with the Bio-Rad ScripTM cDNA Synthesis Kit (catalog number: 1708890, Bio-Rad Laboratories, Hercules, CA, USA) according to the manufacturer's protocols. Quantitative real-time PCR analysis was conducted using SYBR Green Master Mix (catalog number: RR820A, Takara, Dalian, China) on the Bio-Rad CFX Manager system (Bio-Rad Laboratories). Relative gene expression quantification employed the $2^{-\Delta\Delta CT}$ approach following normalization to β-actin levels. Specific oligonucleotide sequences for amplification are detailed in Table 1.

IF Assay

Immunofluorescence analyses were conducted following established protocols. Cardiac perfusion in mice commenced with ice-cold 0.1 M PBS (catalog number: P1020, Solarbio) followed by 4% paraformaldehyde (PFA) infusion. Excised myocardial specimens were fixed in 4% PFA for 24-hour, cryo-embedded in OCT compound (catalog number: 4583, SAKURA, Tokyo, Japan), and sectioned into 5 µm slices. For cellular analysis, cardiac fibroblasts plated on coverslips were maintained in 37 °C/5% CO_2 culture conditions. After three PBS washes, cells were fixed with 4% PFA in room temperature for 15 minutes. Following the restoration with sodium citrate buffer (pH 6.0, catalog number: CP0081, Beyotime) at 94 °C for 15 min, both tissue sections and cellular preparations underwent sequential processing with: BSA blocking solution (catalog number: SW3015, Solarbio), 0.2% Triton X-100 (catalog number: T8200, Solarbio), and specific primary antibodies - TRIM34 (1:100 dilution, catalog number: bs-9244R, Bioss), α-SMA (1:500 dilution, catalog number: ab124964, Abcam), and HNRNPL (1:500 dilution, catalog number: 18354-1-AP, Proteintech, Chicago, IL, USA). Following overnight incubation at 4 °C with primary antibodies, both tissue sections and CFs were rinsed with PBS three times. Secondary antibody treatment involved either Alexa Fluor® 647-conjugated Goat Anti-Rabbit IgG (1:500 dilution, catalog number: ab150083, Abcam) or Alexa Fluor® 488-labeled Goat Anti-Rabbit IgG (1:1000 dilution, catalog number: ab150077, Abcam), applied for 60 minutes at ambient temperature. Specimens were subsequently mounted using DAPI-embedded antifade medium (catalog number: S2110, Solarbio) and imaged using an Olympus IX71 fluorescence microscope system.

Western Blot Analysis

Cardiac tissues and CFs underwent protein extraction using RIPA lysis buffer (catalog number: R0010, Solarbio). Protein concentrations were quantified via BCA assay (catalog number: PC0020, Solarbio), with subsequent separation of 20 µg samples using 10% SDS-PAGE electrophoresis. Separated proteins were electrotransferred onto PVDF membranes (catalog number: IPVH00010, Millipore, Billerica, MA, USA) followed by 1-hour blocking with 5% BSA solution (catalog number: SW3015, Solarbio) at ambient temperature. Membranes underwent overnight incubation with primary antibodies at 4 °C, followed by 1-hour exposure to HRP-conjugated secondary antibodies (1:20,000 dilution, catalog number: ab6721, Abcam). Protein bands were visualized using BeyoECL Plus substrate (catalog number: P0018S, Beyotime), with subsequent densitometric analysis performed through Image-Pro Plus 6.0 (Media Cybernetics, Rockville, MD, USA). The primary antibodies included anti-TRIM34 antibody (1:2000, catalog number: bs-9244R, Bioss), anti-collagen I antibody (1:1000, catalog number: ab21286, Abcam), anti-collagen III antibody (1:1000, catalog number: ab184993, Abcam), anti-alpha smooth muscle actin (anti-α-SMA) antibody (1:50,000, catalog number: ab124964, Abcam), anti-vimentin antibody (1:1000, catalog number: ab45939, Abcam), anti-discoidin domain receptor 2 (anti-DDR2) antibody (1:1000, catalog number: ab76967, Abcam), anti-tensin antibody (1:1000, catalog number: ab233133, Abcam), anti-HNRNPL antibody (1:10,000, catalog number: ab264340, Abcam), anti-SMAD7 antibody (1:1000, catalog number: ab216428, Abcam), anti-phosphorylated SMAD2 (anti-p-SMAD2) antibody (1:1000, catalog number: ab280888, Abcam), anti-SMAD2 antibody (1:3000, catalog number: ab228765, Abcam), anti-p-SMAD3 antibody (1:2000, catalog number: ab52903, Abcam), anti-

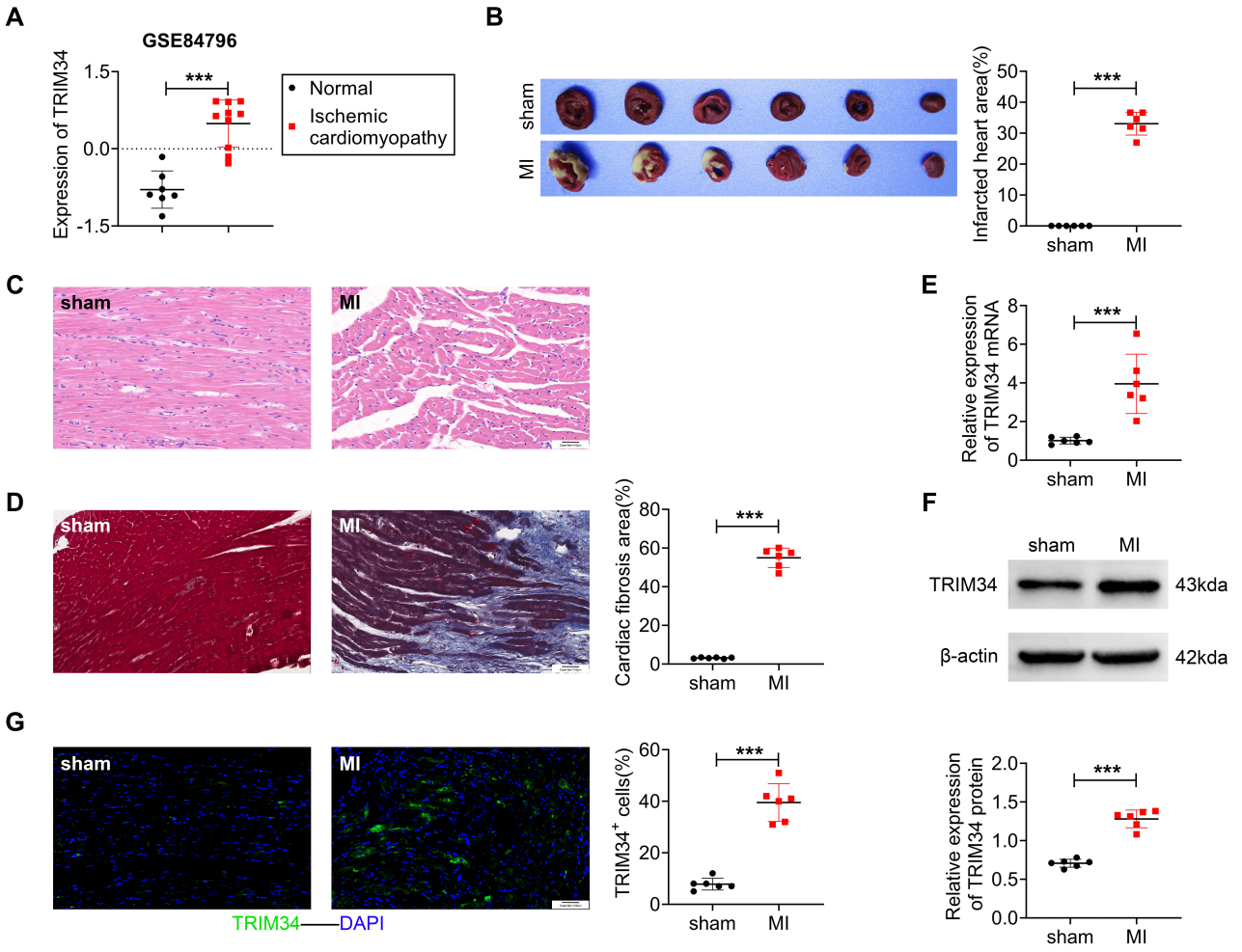

Fig. 1. Upregulated level of TRIM34 in fibrotic tissue of mice. Mice were subjected to MI through ligating the left anterior descending coronary artery to build a model of cardiac fibrosis. (A) The expression of TRIM34 was analyzed based on the GSE84796 microarray dataset. (B) The heart tissues were stained by TTC, and the percentage of infarcted heart area was quantified. (C) Histopathological evaluation was conducted by HE staining, with microscopic observations at 100 µm. (D) The heart tissues were stained by Masson, and the percent of cardiac fibrosis area was quantified. Scale bar = 100 µm. (E) The mRNA expression levels of TRIM34 were quantified through RT-qPCR analysis, with *β-actin* serving as the internal control for data normalization. (F) Protein expression profiles of TRIM34 were assessed using Western blotting, with β-actin normalization applied for comparative analysis. (G) Immunofluorescence staining quantified TRIM34 cellular distribution in cardiac tissues, with positive cell percentages calculated. Scale bar = 100 µm. All measurements were expressed as mean ± SD. n = 6. ***$p < 0.001$.

SMAD3 antibody (1:1000, catalog number: ab84177, Abcam), and anti-β-actin antibody (1:5000, catalog number: ab8227, Abcam).

Statistical Analysis

Statistical analyses were performed using SPSS 20.0 (IBM Corp., Armonk, NY, USA), with experimental data expressed as mean ± standard deviation. The normality and homogeneity of variance of data were analyzed using the Shapiro–Wilk test and Levene's test. All data conformed to normal distribution and homogeneity of variance. Statistical comparisons between two groups were performed using a two-tailed unpaired Student's *t* test, while multi-group comparisons were performed using one-way ANOVA followed by Dunnett's post hoc assessment. Statistical significance was established at p-values < 0.05.

Results

TRIM34 was Highly Expressed in Fibrotic Tissue of Mice

As shown in Fig. 1A, the level of TRIM34 was markedly elevated in patients with heart tissue from end-stage heart failure compared with that in healthy hearts based on the GSE84796 microarray dataset ($p < 0.001$). To address the role of TRIM34 in cardiac fibrosis, mice

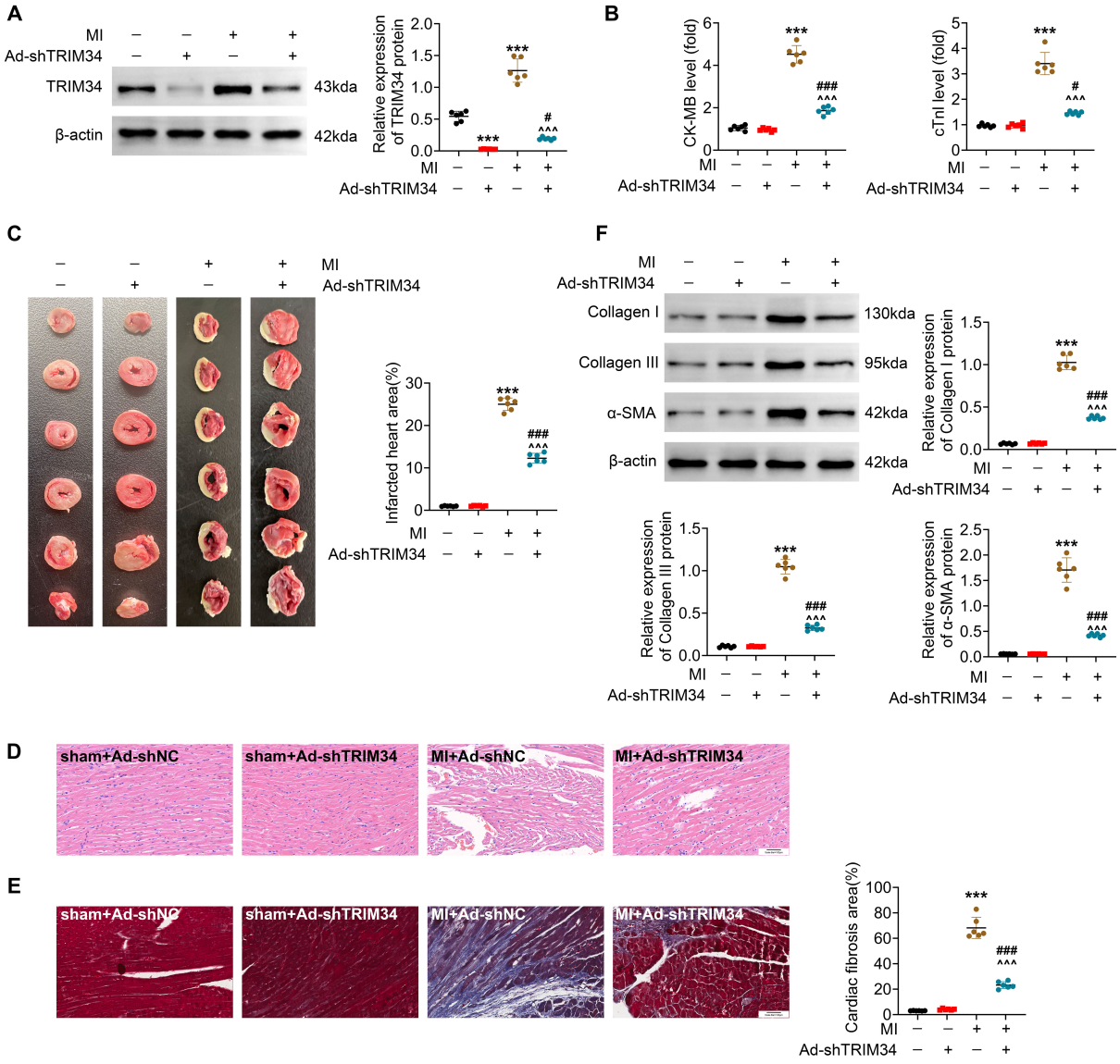

Fig. 2. Knockdown of TRIM34 alleviated cardiac injury and fibrosis in mice. Mice were subjected to MI through ligating the left anterior descending coronary artery to build a model of cardiac fibrosis, and then intramyocardially injected with shTRIM34 to downregulate the level of TRIM34. (A) Protein expression profiles of TRIM34 were assessed using Western blotting, with β-actin normalization applied for comparative analysis. (B) The serum level of CK-MB and cTnl was measured to assess the myocardial damage. (C) The heart tissues were stained by 2,3,5-Triphenyltetrazolium chloride (TTC), and the percentage of infarcted heart area was quantified. (D) Histopathological evaluation was conducted through HE staining, with microscopic observations at 100 µm. (E) The heart tissues were stained by Masson, and the percentage of cardiac fibrosis area was quantified. Scale bar = 100 µm. (F) Protein expression profiles of collagen I, collagen III and α-SMA were assessed using Western blotting, with β-actin normalization applied for comparative analysis. All measurements were expressed as mean $\pm$ SD. n = 6. ***$p < 0.001$ *vs.* control group (without MI and Ad-shTRIM34); #$p < 0.05$ and ###$p < 0.001$ *vs.* Ad-shTRIM34 group; ^^^$p < 0.001$ *vs.* MI group. CK-MB, creatine kinase myocardial band.

were subjected to MI via ligating the left anterior descending coronary artery. The results from Fig. 1B showed that the percent of infarcted heart area in MI mice was signally higher than in sham mice ($p < 0.001$). The myocardial tissue in the MI group showed loss of normal structure and integrity, myocardial fiber disorder and rupture, excessive inflammatory cells infiltrated around the injured cardiomyocytes, and an increase in cardiomyocyte cross-sectional area (CSA) compared with the sham group (Fig. 1C). Besides, a higher percent of cardiac fibrosis area was found in MI mice than that in sham mice (Fig. 1D, $p < 0.001$). The expression of TRIM34 at both the transcriptional and

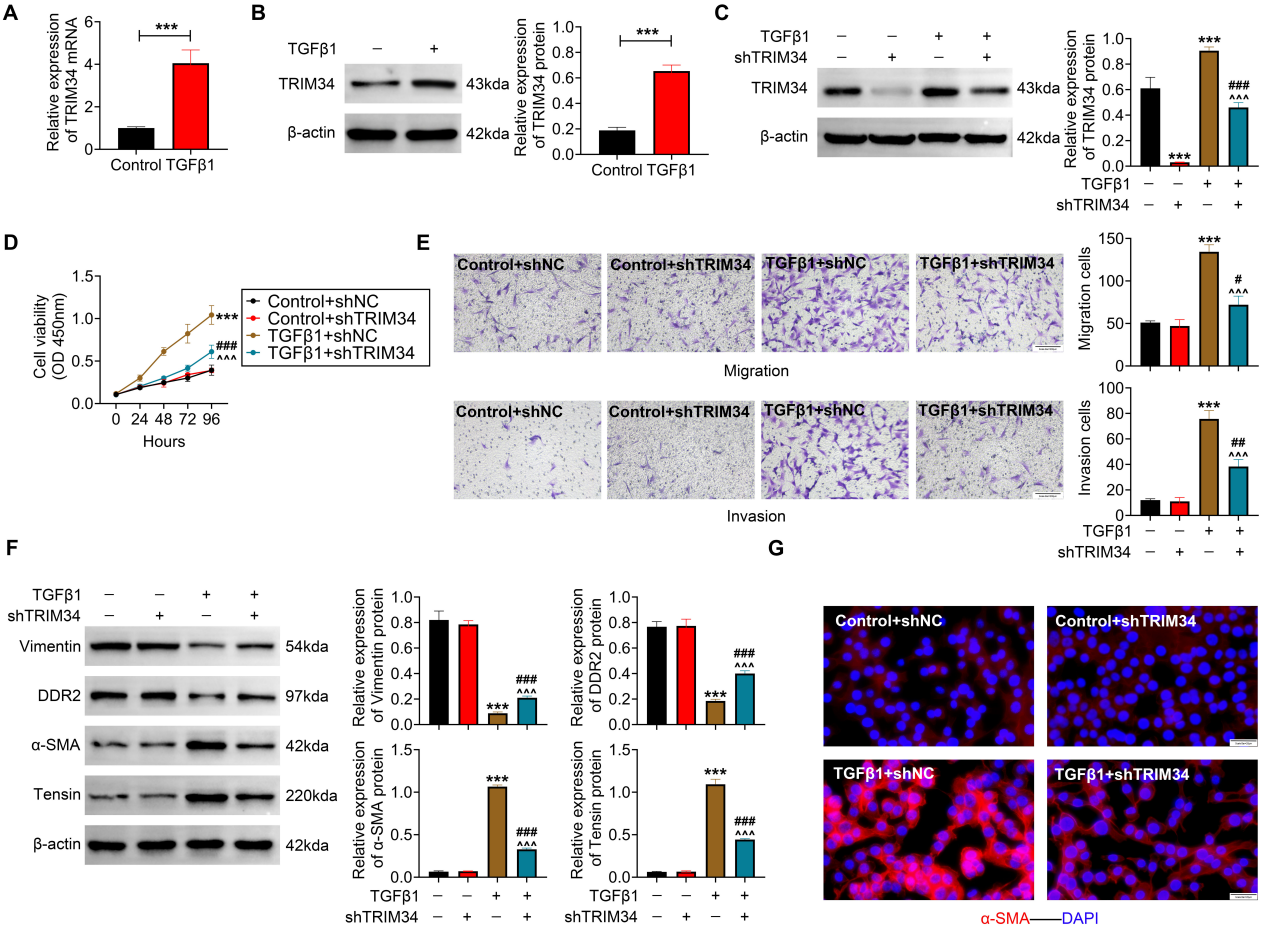

Fig. 3. Knockdown of TRIM34 suppressed the differentiation of fibroblast to myofibroblast *in vitro*. Cardiac fibroblasts (CFs) were exposed to 20 ng/mL TGF-β1 for 24 hours to establish an *in vitro* fibrotic model. (A) The mRNA expression levels of TRIM34 were quantified using RT-qPCR analysis, with *β-actin* serving as the internal control for data normalization. ***$p < 0.001$. (B) Protein expression profiles of TRIM34 were assessed using Western blotting, with β-actin normalization applied for comparative analysis. ***$p < 0.001$. (C) Protein expression profiles of TRIM34 were assessed using Western blotting, with β-actin normalization applied for comparative analysis. ***$p < 0.001$ *vs.* control group (without TGF-β1 and shTRIM34); ###$p < 0.001$ *vs.* shTRIM34 group; ^^^$p < 0.001$ *vs.* TGF-β1 group. (D) The cell viability of CFs was measured using CCK-8 assays. ***$p < 0.001$ *vs.* control group (without TGF-β1 and shTRIM34); ###$p < 0.001$ *vs.* shTRIM34 group; ^^^$p < 0.001$ *vs.* TGF-β1 group. (E) The migration and invasion of CFs were evaluated using Transwell assays, and the numbers of migrated and invaded cells were counted. Scale bar = 200 µm. ***$p < 0.001$ *vs.* control group (without TGF-β1 and shTRIM34); #$p < 0.05$ and ##$p < 0.01$ *vs.* shTRIM34 group; ^^^$p < 0.001$ *vs.* TGF-β1 group. (F) Protein expression profiles of vimentin, DDR2, α-SMA and tensin were assessed using Western blotting, with β-actin normalization applied for comparative analysis. ***$p < 0.001$ *vs.* control group (without TGF-β1 and shTRIM34); ###$p < 0.001$ *vs.* shTRIM34 group; ^^^$p < 0.001$ *vs.* TGF-β1 group. (G) The level of α-SMA was determined using IF assays. Scale bar = 25 µm. All measurements were expressed as mean ± SD. n = 3.

translational levels were significantly enhanced in MI mice (Fig. 1E,F, $p < 0.001$). Moreover, a noteworthy elevation in the percent of TRIM34$^+$ cells was observed in MI mice (Fig. 1G, $p < 0.001$). Thus, the TRIM34 level was upregulated in the fibrotic tissue of mice.

Knockdown of TRIM34 Relieved Cardiac Fibrosis in MI Mice

To dissect the role of TRIM34 in cardiac fibrosis, shRNA targeting TRIM34 was constructed to downregulate the TRIM34 level in MI mice. Treatment of shTRIM34 significantly reduced the TRIM34 expression in sham and MI mice (Fig. 2A, $p < 0.001$), but the expression of TRIM34 in MI mice treated with shTRIM34 was dramatically increased compared to that in sham mice with shTRIM34

(Fig. 2A, $p < 0.05$). A remarkable elevation in the levels of CK-MB and cTnl was found in MI mice, which was significantly declined following shTRIM34 treatment (Fig. 2B, $p < 0.001$). Also, treatment of shTRIM34 significantly decreased the MI-induced elevation in the percent of infarcted heart area (Fig. 2C, $p < 0.001$) and the pathological damage in heart tissues (Fig. 2D). Besides, treatment of shTRIM34 prominently decreased the percentage of cardiac fibrosis area in MI mice (Fig. 2E, $p < 0.001$). The relative protein expression of collagen I, collagen III and α-SMA was markedly elevated in MI mice, which was notably counteracted with the administration of shTRIM34 (Fig. 2F, $p < 0.001$). Totally, silencing of TRIM34 alleviated cardiac damage and fibrosis in mice.

Knockdown of TRIM34 Inhibited the Differentiation of Fibroblasts to Myofibroblasts In Vitro

Moreover, CFs were induced with TGF-β1 to construct the *in vitro* model of cardiac fibrosis and to study the role of TRIM34 in cardiac fibrosis. TGF-β1 treatment led to a conspicuous elevation in the transcriptional and translational expression of TRIM34 (Fig. 3A,B, $p < 0.001$). Transfection of shTRIM34 markedly reduced the TRIM34 expression in CFs and TGF-β1-exposed CFs, but the TRIM34 level in TGF-β1-induced CFs was significantly higher than that in CFs (Fig. 3C, $p < 0.001$). TGF-β1-exposure significantly elevated CF cell viability, migration and invasion, which was markedly reduced by transfection with shTRIM34 (Fig. 3D,E, $p < 0.001$). Moreover, the expression level of fibroblast markers (vimentin and DDR2) was significantly decreased, and that of myofibroblast markers (α-SMA and tensin) was notably enhanced in TGF-β1-induced CFs. However, all the changes were reversed with the transfection of shTRIM34 (Fig. 3F, $p < 0.001$). Additionally, transfection of shTRIM34 obviously reduced the α-SMA level in TGF-β1-evoked CFs according to the IF staining (Fig. 3G). Altogether, TRIM34 downregulation suppressed the differentiation of fibroblasts to myofibroblasts *in vitro*.

TRIM34 Promoted Ubiquitination Degradation of HNRNPL

To discover the underlying mechanism of TRIM34 in cardiac fibrosis, the ubiquitinated role of TRIM34 was explored since E3 ubiquitin ligase activity has been demonstrated to be its most prominent feature [20]. Given that HNRNPL was shown to be susceptible to ubiquitin-mediated proteolysis [15], we investigated whether TRIM34 could promote HNRNPL degradation via ubiquitination. HNRNPL was upregulated in MI mice and TGF-β1-exposed CFs at the translational level, which was reduced with knockdown of TRIM34 (Fig. 4A,B, $p < 0.001$). The HNRNPL level in MI mice administered with shTRIM34 was significantly higher than that in sham mice injected with shTRIM34, and similar results were observed *in vitro* (Fig. 4A,B, $p < 0.05$). The interaction of TRIM34 and HNRNPL was revealed through Co-IP assays (Fig. 4C), and the co-localization between TRIM34 and HNRNPL was elucidated via IF analysis in CFs (Fig. 4D). A significant reduction of K63-linked ubiquitination in HNRNPL immunoprecipitates was found in CFs transfected with shTRIM34 (Fig. 4E). After the treatment of CHX, the degradation of endogenous HNRNPL was shown to be down-regulated in CFs transfected with shTRIM34 in a time-dependent way (Fig. 4F, $p < 0.001$), suggesting that knockdown of TRIM34 promoted the protein stability of HNRNPL. Altogether, TRIM34 contributed to the ubiquitination degradation of HNRNPL.

TRIM34 Regulated the Transcription of the SMAD7 Promoter by Suppressing the Level of HNRNPL

Since HNRNPL can promote the transcription of SMAD7, which causes the inhibition of the TGFβ-SMAD signaling pathway [13]. SMAD7 has been revealed to prevent post-infarction HF by attenuating the activation of myofibroblasts and reducing the synthesis of extracellular matrix proteins in structural and stromal cells [14]. Thus, to further resolve the potential mechanism of TRIM34 in cardiac fibrosis, the expression of SMAD7 was examined in MI mice and TGF-β1-exposed CFs. The relative mRNA and protein expression of SMAD7 was reduced in MI mice and TGF-β1-exposed CFs, which was significantly restored after the knockdown of TRIM34 (Fig. 5A–D, $p < 0.05$). Besides, the relative mRNA and protein expression of SMAD7 in MI mice administered with shTRIM34 was notably lower than that in sham mice injected with shTRIM34, and similar results were found *in vitro* (Fig. 5A–D, $p < 0.001$). In addition, the expression of proteins involved in the TGFβ-SMAD signaling axis was revealed by Western blotting. The relative level of p-SMAD2/SMAD2 and p-SMAD3/SMAD3 was observably elevated in MI mice and TGF-β1-exposed CFs (Fig. 5B,D, $p < 0.05$), which was significantly neutralized after the TRIM34 knockdown (Fig. 5B,D, $p < 0.01$). To further confirm the regulative role of TRIM34 in SMAD7, the luciferase plasmids including SMAD7 promoter sequences of different lengths were constructed for the promoter luciferase assays. No statistical difference in the luciferase activity was observed between co-transfection of shNC and empty vector plasmids and co-transfection of shTRIM34 and empty vector plasmids into CFs (Fig. 5E, $p > 0.05$). Also, no statistical difference in the luciferase activity was observed between co-transfection of shNC and the –200 nt to +200 nt region of the SMAD7 promoter and those co-transfected with shTRIM34 and the same promoter construct (Fig. 5E, $p > 0.05$). However, a markedly elevated luciferase activity was found in CFs co-transfected with shTRIM34 and SMAD7 promoter constructs spanning–500-nt to +200-nt, –800-nt to +200-nt, –1200-nt to +200-nt, –1600-nt to +200-nt, and –2000-nt to +200-nt, compared with CFs co-transfected with shNC

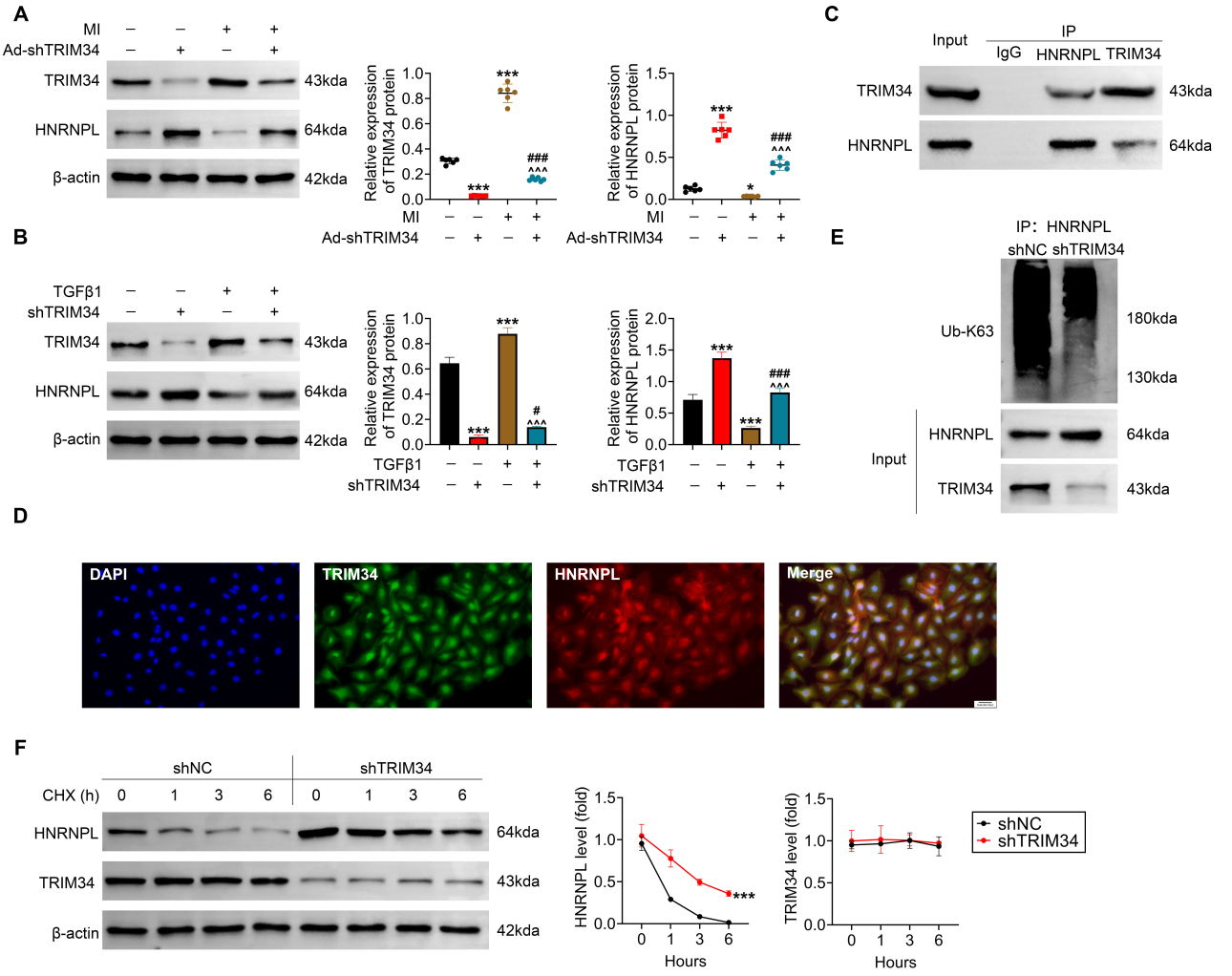

Fig. 4. TRIM34 accelerated ubiquitination degradation of HNRNPL. (A) Protein expression profiles of TRIM34 and HNRNPL were assessed using Western blotting, with β-actin normalization applied for comparative analysis. *$p < 0.05$ and ***$p < 0.001$ *vs.* control group (without MI and Ad-shTRIM34); ###$p < 0.001$ *vs.* Ad-shTRIM34 group; ^^^$p < 0.001$ *vs.* MI group. (B) Protein expression profiles of TRIM34 and HNRNPL were assessed using Western blotting, with β-actin normalization applied for comparative analysis. ***$p < 0.001$ *vs.* control group (without TGF-β1 and shTRIM34); #$p < 0.05$ and ###$p < 0.001$ *vs.* shTRIM34 group; ^^^$p < 0.001$ *vs.* TGF-β1 group. (C) The interaction of TRIM34 and HNRNPL was identified using Co-IP assays in CFs. (D) Immunofluorescence analysis confirmed the co-localization of TRIM34 and HNRNPL in CFs. Scale bar = 25 μm. (E) Ubiquitin modification status of HNRNPL was evaluated in CF cultures. (F) Cycloheximide (CHX) treatment was used to assess HNRNPL protein stability dynamics in CFs. ***$p < 0.001$ *vs.* shTRIM34. Data were shown as mean ± SD. n = 6 (in mice) or 3 (in CFs).

and the corresponding promoter constructs (Fig. 5E, $p < 0.01$). Thus, these results suggested that knockdown of TRIM34 in CFs increased the luciferase activity, and the -500-nt to -200-nt region of the SMAD7 promoter significantly enhanced the luciferase activity in CFs transfected with shTRIM34, indicating an important role of this region in TRIM34-mediated SMAD7 transactivation. However, the direct interaction between TRIM34 and SMAD7 was not detected through ChIP-qPCR assays (Fig. 5F), suggesting that TRIM34 might be indirect in regulating SMAD7 transcription. Additionally, HNRNPL overexpression significantly increased the relative SMAD7 promoter luciferase activity (Fig. 5G, $p < 0.001$), and the combination of HNRNPL overexpression and TRIM34 knockdown further elevated the relative SMAD7 promoter luciferase activity (Fig. 5G, $p < 0.01$). The results indicated that HNRNPL directly bound to the SMAD7 promoter, and TRIM34 enhanced SMAD7 promoter activity through HNRNPL, which was further verified by ChIP-qPCR assays (Fig. 5H, $p < 0.01$). Furthermore, the relative mRNA expression of SMAD7 in CFs was notably elevated with transfection of shTRIM34, which was notably offset with the shHNRNPL administration (Fig. 5I, $p < 0.001$). Besides, the relative mRNA expression of

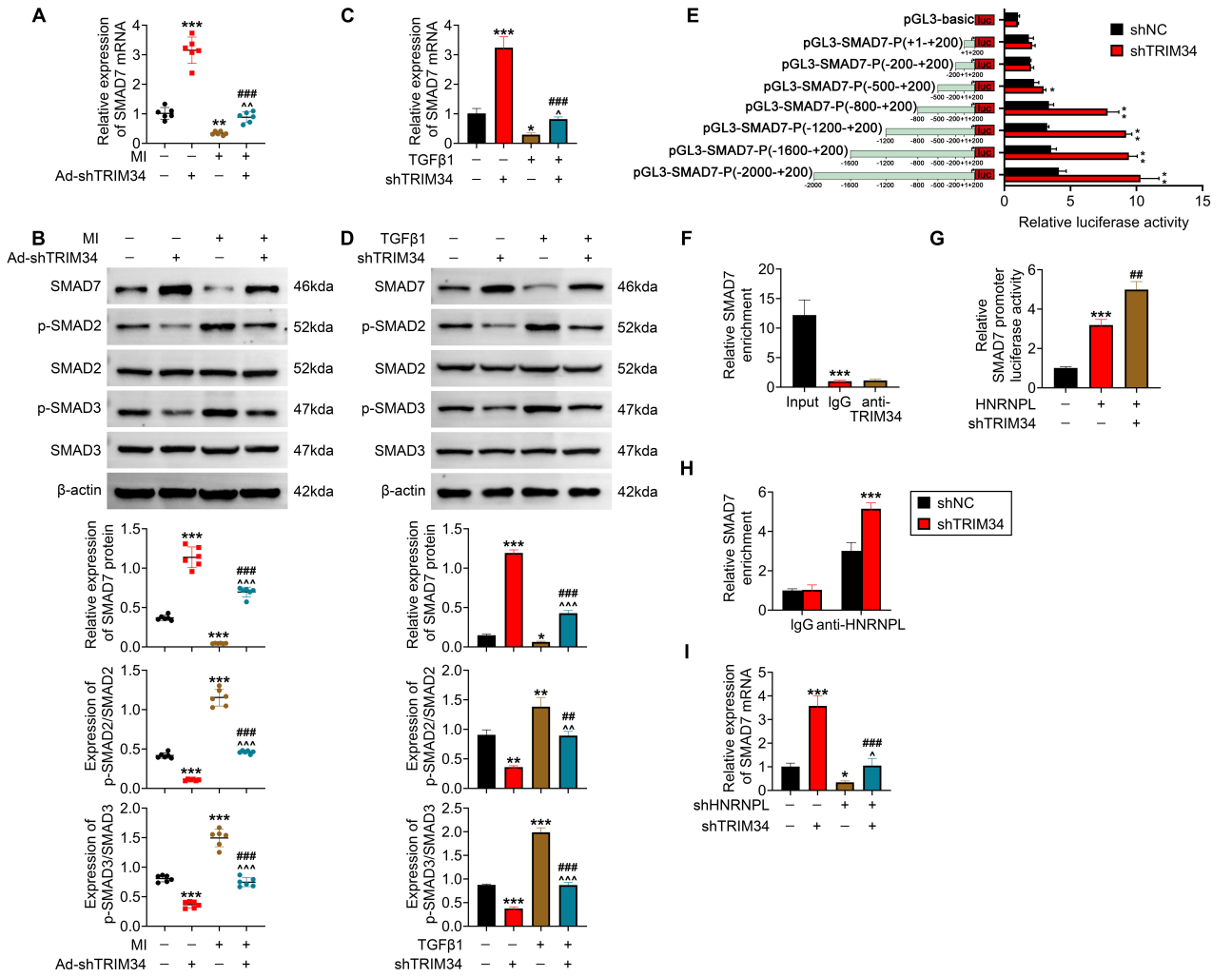

Fig. 5. TRIM34 modulated the transcription of the SMAD7 promoter by inhibiting the expression of HNRNPL. (A) The mRNA expression levels of SMAD7 were quantified through RT-qPCR analysis, with *β-actin* serving as the internal control for data normalization. $^{**}p < 0.01$ and $^{***}p < 0.001$ *vs.* control group (without MI and Ad-shTRIM34); $^{\#\#\#}p < 0.001$ *vs.* Ad-shTRIM34 group; $^{\wedge\wedge}p < 0.01$ *vs.* MI group. (B) Western blotting detected expression patterns of SMAD7, SMAD2, phosphorylated SMAD2, SMAD3, and phosphorylated SMAD3 in cardiac tissues. Results were calculated relative to *β*-actin expression levels for standardized comparison. $^{***}p < 0.001$ *vs.* control group (without MI and Ad-shTRIM34); $^{\#\#\#}p < 0.001$ *vs.* Ad-shTRIM34 group; $^{\wedge\wedge\wedge}p < 0.001$ *vs.* MI group. (C) The mRNA expression levels of SMAD7 were quantified using RT-qPCR analysis, with *β-actin* serving as the internal control for data normalization. $^{*}p < 0.05$ and $^{***}p < 0.001$ *vs.* control group (without TGF-*β*1 and shTRIM34); $^{\#\#\#}p < 0.001$ *vs.* shTRIM34 group; $^{\wedge}p < 0.05$ *vs.* TGF-*β*1 group. (D) Western blotting detected expression patterns of SMAD7, SMAD2, phosphorylated SMAD2, SMAD3, and phosphorylated SMAD3 in CFs. Results were calculated relative to *β*-actin expression levels for standardized comparison. $^{*}p < 0.05$, $^{**}p < 0.01$ and $^{***}p < 0.001$ *vs.* control group (without TGF-*β*1 and shTRIM34); $^{\#\#}p < 0.01$ and $^{\#\#\#}p < 0.001$ *vs.* shTRIM34 group; $^{\wedge\wedge}p < 0.01$ and $^{\wedge\wedge\wedge}p < 0.001$ *vs.* TGF-*β*1 group. (E) The transcriptional activity of SMAD7 in TRIM34-downregulating CFs transfected with truncated SMAD7 promoter luciferase plasmids. $^{*}p < 0.05$ and $^{**}p < 0.01$ *vs.* shNC. (F) The TRIM34-related chromatin fragments of the SMAD7 promoter were examined by ChIP-qPCR assays, with *β-actin* serving as the internal control for data normalization. $^{***}p < 0.001$ *vs.* input. (G) The luciferase activity of CFs. $^{***}p < 0.001$ *vs.* control group (without HNRNPL and shTRIM34); $^{\#\#}p < 0.01$ *vs.* HNRNPL group. (H) The HNRNPL-related chromatin fragments of the SMAD7 promoter were examined by ChIP-qPCR assays, with *β-actin* serving as the internal control for data normalization. $^{***}p < 0.001$ *vs.* shNC. (I) The relative mRNA expression of SMAD7 in CFs transfected with shTRIM34 and/or shHNRNPL was determined by RT-qPCR, with *β-actin* serving as the internal control for data normalization. $^{*}p < 0.05$ and $^{***}p < 0.001$ *vs.* control group (without shHNRNPL and shTRIM34); $^{\#\#\#}p < 0.001$ *vs.* shTRIM34 group; $^{\wedge}p < 0.05$ *vs.* shHNRNPL group. Data were shown as mean ± SD. n = 6 (in mice) or 3 (in CFs).

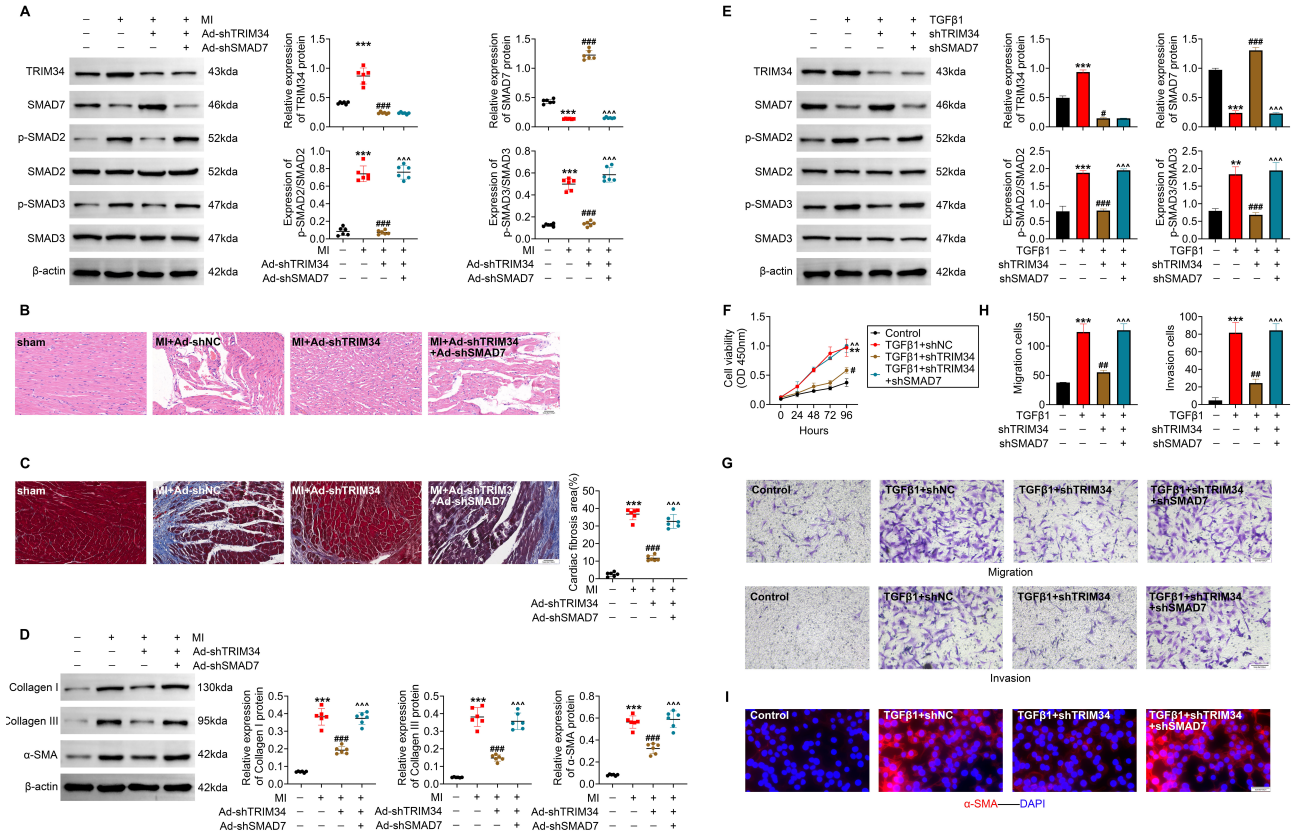

Fig. 6. The suppressive role of the TRIM34 knockdown in cardiac fibrosis was neutralized with the silencing of SMAD7, both *in vivo* and *in vitro*. (A) Western blotting detected expression patterns of SMAD7, SMAD2, phosphorylated SMAD2, SMAD3, and phosphorylated SMAD3 in cardiac tissues. Results were calculated relative to β-actin expression levels for standardized comparison. ***$p < 0.001$ *vs.* control group (without MI, Ad-shTRIM34 and Ad-shSMAD7); ###$p < 0.001$ *vs.* MI group; ^^^$p < 0.001$ *vs.* MI+Ad-shTRIM34 group. (B) Histopathological evaluation was conducted through HE staining, with microscopic observations at 100 μm. (C) The heart tissues were stained by Masson, and the percentage of cardiac fibrosis area was quantified. Scale bar = 100 μm. ***$p < 0.001$ *vs.* control group (without MI, Ad-shTRIM34 and Ad-shSMAD7); ###$p < 0.001$ *vs.* MI group; ^^^$p < 0.001$ *vs.* MI+Ad-shTRIM34 group. (D) The relative protein expression of collagen I, collagen III and α-SMA was determined by Western blotting. Data were presented after being normalized with β-actin. ***$p < 0.001$ *vs.* control group (without MI, Ad-shTRIM34 and Ad-shSMAD7); ###$p <$ 0.001 *vs.* MI group; ^^^$p < 0.001$ *vs.* MI+Ad-shTRIM34 group. (E) Western blotting detected expression patterns of SMAD7, SMAD2, phosphorylated SMAD2, SMAD3, and phosphorylated SMAD3 in CFs. Results were calculated relative to β-actin expression levels for standardized comparison. **$p < 0.01$ and ***$p < 0.001$ *vs.* control group (without TGF-β1, shTRIM34 and shSMAD7); #$p < 0.05$ and ###$p < 0.001$ *vs.* TGF-β1 group; ^^^$p < 0.001$ *vs.* TGF-β1+shTRIM34 group. (F) The cell viability of CFs was measured with CCK-8 assays. **$p < 0.01$ *vs.* control group (without TGF-β1, shTRIM34 and shSMAD7); #$p < 0.05$ *vs.* TGF-β1 group; ^^$p < 0.01$ *vs.* TGF-β1+shTRIM34 group. (G,H) The migration and invasion of CFs were evaluated by Transwell assays, and the numbers of migrated and invaded cells were counted. Scale bar = 200 μm. ***$p < 0.001$ *vs.* control group (without TGF-β1, shTRIM34 and shSMAD7); ##p < 0.01 *vs.* TGF-β1 group; ^^^$p < 0.001$ *vs.* TGF-β1+shTRIM34 group. (I) The level of α-SMA was determined by IF assays. Scale bar = 25 μm. Data were shown as mean ± SD. n = 6 (in mice) or 3 (in CFs).

SMAD7 in CFs was markedly declined with the introduction of shHNRNPL, which was notably reversed following the treatment of shTRIM34 (Fig. 5I, $p < 0.05$). Collectively, TRIM34 indirectly regulated the transcription of the SMAD7 promoter by inhibiting the expression of HNRNPL.

Downregulation of SMAD7 Reversed the Antifibrotic Role of Knockdown TRIM34

To further confirm the action of the TRIM34/HNRNPL/SMAD7 axis in cardiac fibrosis, the rescue assay was conducted by knockdown of HNRNPL or SMAD7 *in vivo* and *in vitro*. A prominent increase in the TRIM34 level was observed in heart tissues from MI mice, which was notably declined with

the shTRIM34 (**Supplementary Fig. 1A** and Fig. 6A, $p < 0.001$). However, no influence on the expression of TRIM34 was found by further downregulating the level of HNRNPL or SMAD7 in MI mice treated with shTRIM34 (**Supplementary Fig. 1A** and Fig. 6A, $p > 0.05$). Management of shTRIM34 prominently rescued the level of SMAD7 in heart tissues from MI mice, which was reversed following the shSMAD7 treatment (Fig. 6A, $p < 0.001$). Similarly, injection of shTRIM34 markedly recovered the level of HNRNPL in heart tissues, which was inverted with the shHNRNPL treatment (**Supplementary Fig. 1A**, $p < 0.001$). Besides, administration of shTRIM34 significantly reduced the relative level of p-SMAD2/SMAD2 and p-SMAD3/SMAD3 in heart tissues, which was observably restored with the injection of shSMAD7 (Fig. 6A, $p < 0.001$). Also, the ameliorative role of shTRIM34 in pathological symptoms was distinctly effaced with the treatment of shHNRNPL or shSMAD7 (**Supplementary Fig. 1B** and Fig. 6B). The inhibitory role of shTRIM34 in the percent of cardiac fibrosis area, and the level of collagen I, collagen III and α-SMA in MI mice was prominently vanished with the administration of shHNRNPL or shSMAD7 (**Supplementary Fig. 1C**,**D**, as well as Fig. 6C,D, $p < 0.001$). In addition, TGF-β1 induced a remarkable enhancement in the expression of TRIM34, which was reduced with the transfection of shTRIM34 but not shHNRNPL or shSMAD7 (**Supplementary Fig. 2A** and Fig. 6E, $p < 0.05$). Introduction of shTRIM34 prominently restored the expression of SMAD7 in TGF-β1-induced CFs, which was inverted with the transfection of shSMAD7 (Fig. 6E, $p < 0.001$). Also, treatment of shTRIM34 significantly rescued the expression of HNRNPL in TGF-β1-induced CFs, which was reversed with the transfection of shHNRNPL (**Supplementary Fig. 2A**, $p < 0.001$). Reverse results were observed in the level of p-SMAD2/SMAD2 and p-SMAD3/SMAD3 (Fig. 6E, $p < 0.01$). Additionally, administration of shTRIM34 markedly decreased the cell viability, migration cell numbers, invasion cell numbers, and the level of α-SMA in TGF-β1-induced CFs, which was observably recovered with the treatment of shHNRNPL or shSMAD7 (**Supplementary Fig. 2A–C**, and Fig. 6F–I, $p < 0.05$). Altogether, the antifibrotic role of shSMAD7 was counteracted with the knockdown of shHNRNPL or SMAD7 both in MI mice and TGF-β1-exposed CFs, indicating a direct role of the TRIM34-HNRNPL-SMAD7 pathway in MI.

Discussion

The model of cardiac fibrosis was established in mice with MI *in vivo* and CFs with TGF-β1 *in vitro* to explore the action of TRIM34 in the transformation of cardiac fibroblasts to myofibroblasts in this research. Upregulation of TRIM34 was found in fibrotic tissue of mice and TGF-β1-exposed CFs. TRIM34 silencing reduced the level of myocardial damage markers, the infarcted heart area, and the pathological symptoms, as well as the cardiac fibrosis area, and the expression of fibrosis markers in MI mice. Additionally, downregulation of TRIM34 declined the cell viability, numbers of migrated and invaded cells, and the level of myofibroblast markers, but elevated the level of fibroblast markers in TGF-β1-induced CFs. Moreover, TRIM34 directly interacted and promoted ubiquitination degradation of HNRNPL. Furthermore, HNRNPL directly bound to the SMAD7 promoter, and TRIM34 indirectly regulated the transcription of the SMAD7 promoter by inhibiting the expression of HNRNPL. Rescue experiments showed that knockdown of HNRNPL and SMAD7 counteracted the antifibrotic role of shTRIM34 in MI mice and TGF-β1-exposed CFs. Altogether, TRIM34 induced cardiac fibrosis via promoting the ubiquitination degradation of HNRNPL to indirectly regulate the transcription of SMAD7.

The model of MI in animals is a representative experimental tool for precisely investigating the spatiotemporal alterations of CF populations during cardiac repair [21]. Surgical ligation of LAD results in the fast death of cardiomyocytes in the ischemic left ventricle and the progressive generation of different myocardial areas, including the infarct and remote zones [22]. The infarct regions primarily experience replacement fibrosis that can restrain ventricular rupture initially. However, if left untreated, replacement fibrosis can drive the progression of non-compliant and ECM-rich scars that deteriorate over time in heart function. Inversely, the remote areas visually resemble the healthy myocardium, but reactive fibrosis still occurs [22]. TGF-β1 is a powerful contributor to cardiac fibrosis, which has been widely used for the construction of cardiac fibrosis *in vitro* [17]. Consistently, this study established the model of cardiac fibrosis in mice with MI and CFs with TGF-β1 to explore the role of TRIM34 in the transformation of cardiac fibroblast to myofibroblast, aligning with the previous studies [17,21]. Upregulation of TRIM34 through interferon is revealed to be involved in the defense against infections [23]. Notably, TRIM34 is identified as the hub gene in persistent atrial fibrillation [24]. Similar to these findings, the present study found that the level of TRIM34 was elevated *in silicon*, *in vitro* and *in vivo*. Knockdown of TRIM34 reduced the cardiac fibrosis areas and the level of fibrosis markers, containing collagen I, collagen III and α-SMA in MI mice. Additionally, knockdown of TRIM34 reduced the cell viability, numbers of migrated and invaded cells, and the level of myofibroblast markers (α-SMA and tensin), with an increased level of fibroblast markers (vimentin and DDR2) [25] in TGF-β1-induced CFs. Taken together, upregulation of TRIM34 promoted cardiac fibrosis *in vivo* and *in vitro*.

The most pronounced feature of TRIM34 is the E3 ubiquitin ligase activity. The K63-linked polyubiquitination role of TRIM34 in ZBP1 has been revealed to regu-

late influenza virus-activated programmed cell death [20]. Moreover, TRIM34 has been identified as one of the genes involved in the E3-related prognostic signature in gliomas [26]. Similarly, TRIM34 directly bound and promoted ubiquitination degradation of HNRNPL in this study. HNRNPL is related to splicing efficiency and nitric oxide synthesis in cardiac diseases [27], as well as the progression of MI [28], which can be easily degraded by ubiquitin-mediated proteolysis [15]. Furthermore, HNRNPL directly bound to the SMAD7 promoter, in line with the previous results [13]. However, this study found that TRIM34 suppressed the transcription of the SMAD7 promoter by inhibiting the expression of HNRNPL, not directly suppressing the function of SMAD7, which further promoted the expression of the TGFβ-SMAD signaling pathway. SMAD7 has been demonstrated to restrain post-infarction HF by reducing the activation of myofibroblasts and the synthesis of extracellular matrix proteins in structural and stromal cells [14]. SMAD7 is an endogenous negative modulator of the TGFβ-SMAD signaling that suppresses the TGFβ receptor-mediated SMAD phosphorylation, thus preventing the transcription of downstream profibrotic genes [29]. The TGFβ-SMAD signaling pathway plays a significant role in cardiac fibrosis and can be a potential therapeutic target for cardiac fibrosis based on the multiple studies [30–35]. Thus, rescue experiments showed that knockdown of HNRNPL or SMAD7 counteracted the antifibrotic role of shTRIM34 in MI mice and TGF-β1-exposed CFs. Therefore, TRIM34 evoked cardiac fibrosis by promoting the ubiquitination degradation of HNRNPL to indirectly regulate the transcription of SMAD7.

Conclusion

In summary, the expression of TRIM34 was increased in MI mice and TGF-β1-elicited CFs. TRIM34 silencing prevented cardiac fibrosis both *in vivo* and *in vitro*. Mechanically, TRIM34 enhanced the ubiquitination degradation of HNRNPL to indirectly regulate the transcription of SMAD7, thereby promoting the expression of the TGFβ-SMAD signaling pathway. However, more clinical characteristics of TRIM34 can be analyzed in the future. Secondly, more shRNAs targeting TRIM34, HNRNPL and SMAD7 can be synthesized and used for the experiments to exclude the off-target effect. Additionally, more preclinical and clinical assays are necessary in the following study. Besides, accurate quantification of cardiac fibrosis should be based on full-field transverse heart sections; therefore, images of the entire heart are recommended. However, the whole-heart images were not captured due to an oversight during the experiment, which is a limitation of this study. Furthermore, cardiac echocardiography results were not included due to technical, equipment and financial constraints. Despite these limitations, the results can provide valuable insights into the mechanisms underlying cardiac fibrosis and may contribute to the development of potential therapeutic strategies.

Availability of Data and Materials

All experimental datasets supporting this research are either contained within this publication or obtainable through reasonable request to the corresponding author.

Author Contributions

YH designed the study, completed the experiment and supervised the data collection. BW analyzed the data and interpreted the data. YH wrote the first draft and prepared the manuscript for publication. BW reviewed the manuscript draft and contributed to important revisions. Both authors have read and approved the manuscript. Both authors gave final approval of the version to be published. Both authors have participated sufficiently in the work to take public responsibility for appropriate portions of the content and agreed to be accountable for all aspects of the work in ensuring that questions related to its accuracy or integrity.

Ethics Approval and Consent to Participate

Animal experiments were conducted in compliance with the Guide for the Care and Use of Laboratory Animals [16] and approved by the Animal Research Ethics Committee of the Second Affiliated Hospital of Soochow University (Approval No. EC2022(131)).

Acknowledgment

Not applicable.

Funding

This work was supported by Suzhou Science and Technology Plan Project (Grant No. SKY2022145).

Conflict of Interest

The authors declare no conflict of interest.

Supplementary Material

Supplementary material associated with this article can be found, in the online version, at https://doi.org/10.24976/Discov.Med.202638207.104.

References

[1] Li Y. Novel Therapeutic Strategies Targeting Fibroblasts to Improve Heart Disease. Journal of Cellular Physiology. 2024; 240: e31504. https://doi.org/10.1002/jcp.31504.

[2] González A, Schelbert EB, Díez J, Butler J. Myocardial Interstitial Fibrosis in Heart Failure: Biological and Translational Per-

spectives. Journal of the American College of Cardiology. 2018; 71: 1696–1706. https://doi.org/10.1016/j.jacc.2018.02.021.

[3] Frangogiannis NG. The extracellular matrix in myocardial injury, repair, and remodeling. The Journal of Clinical Investigation. 2017; 127: 1600–1612. https://doi.org/10.1172/JCI87491.

[4] Ong SB, Hernández-Reséndiz S, Crespo-Avilan GE, Mukhametshina RT, Kwek XY, Cabrera-Fuentes HA, *et al*. Inflammation following acute myocardial infarction: Multiple players, dynamic roles, and novel therapeutic opportunities. Pharmacology & Therapeutics. 2018; 186: 73–87. https://doi.org/10.1016/j.pharmthera.2018.01.001.

[5] Hinderer S, Schenke-Layland K. Cardiac fibrosis - A short review of causes and therapeutic strategies. Advanced Drug Delivery Reviews. 2019; 146: 77–82. https://doi.org/10.1016/j.addr.2019.05.011.

[6] Kleinbongard P, Senyo SE, Lindsey ML, Garvin AM, Simpson JA, de Castro Braz LE. Cardiac fibroblasts: answering the call. American Journal of Physiology. Heart and Circulatory Physiology. 2024; 327: H681–H686. https://doi.org/10.1152/ajpheart.00478.2024.

[7] Lunde IG, Rypdal KB, Van Linthout S, Diez J, González A. Myocardial fibrosis from the perspective of the extracellular matrix: Mechanisms to clinical impact. Matrix Biology: Journal of the International Society for Matrix Biology. 2024; 134: 1–22. https://doi.org/10.1016/j.matbio.2024.08.008.

[8] Venuto S, Merla G. E3 Ubiquitin Ligase TRIM Proteins, Cell Cycle and Mitosis. Cells. 2019; 8: 510. https://doi.org/10.3390/cells8050510.

[9] Wan T, Li X, Li Y. The role of TRIM family proteins in autophagy, pyroptosis, and diabetes mellitus. Cell Biology International. 2021; 45: 913–926. https://doi.org/10.1002/cbin.11550.

[10] Shen Z, Wei L, Yu ZB, Yao ZY, Cheng J, Wang YT, *et al*. The Roles of TRIMs in Antiviral Innate Immune Signaling. Frontiers in Cellular and Infection Microbiology. 2021; 11: 628275. https://doi.org/10.3389/fcimb.2021.628275.

[11] Zhao G, Liu C, Wen X, Luan G, Xie L, Guo X. The translational values of TRIM family in pan-cancers: From functions and mechanisms to clinics. Pharmacology & Therapeutics. 2021; 227: 107881. https://doi.org/10.1016/j.pharmthera.2021.107881.

[12] Twentyman J, Khalifeh A, Felton AL, Emerman M, OhAinle M. Primate TRIM34 is a broadly-acting, TRIM5-dependent lentiviral restriction factor. BioRxiv: the Preprint Server for Biology. 2023; 2023.03.24.534139. https://doi.org/10.1101/2023.03.24.534139.

[13] An M, Zheng H, Huang J, Lin Y, Luo Y, Kong Y, *et al*. Aberrant Nuclear Export of circNCOR1 Underlies SMAD7-Mediated Lymph Node Metastasis of Bladder Cancer. Cancer Research. 2022; 82: 2239–2253. https://doi.org/10.1158/0008-5472.CAN-21-4349.

[14] Humeres C, Shinde AV, Hanna A, Alex L, Hernández SC, Li R, *et al*. Smad7 effects on TGF-β and ErbB2 restrain myofibroblast activation and protect from postinfarction heart failure. The Journal of Clinical Investigation. 2022; 132: e146926. https://doi.org/10.1172/JCI146926.

[15] Ji M, Zhao Z, Li Y, Xu P, Shi J, Li Z, *et al*. FBXO16-mediated hnRNPL ubiquitination and degradation plays a tumor suppressor role in ovarian cancer. Cell Death & Disease. 2021; 12: 758. https://doi.org/10.1038/s41419-021-04040-9.

[16] National Research Council Committee for the Update of the Guide for the Care and Use of Laboratory Animals. Guide for the Care and Use of Laboratory Animals. National Academies Press (US): Washington (DC). 2011.

[17] Li T, Zhuang Y, Yang W, Xie Y, Shang W, Su S, *et al*. Silencing of METTL3 attenuates cardiac fibrosis induced by myocardial infarction via inhibiting the activation of cardiac fibroblasts. FASEB Journal: Official Publication of the Federation of American Societies for Experimental Biology. 2021; 35: e21162. https://doi.org/10.1096/fj.201903169R.

[18] Zhao Q, Zhang CL, Xiang RL, Wu LL, Li L. CTRP15 derived from cardiac myocytes attenuates TGFβ1-induced fibrotic response in cardiac fibroblasts. Cardiovascular Drugs and Therapy. 2020; 34: 591–604. https://doi.org/10.1007/s10557-020-06970-6.

[19] Leng X, Hu Z, Zhang M, Chen Q, Xu K, Zhao J. RNF125 suppresses stem cell-like properties and metastasis in non-small cell lung cancer by promoting ubiquitination and degradation of DDX5. Pathology, Research and Practice. 2026; 279: 156378. https://doi.org/10.1016/j.prp.2026.156378.

[20] Wang X, Xiong J, Zhou D, Zhang S, Wang L, Tian Q, *et al*. TRIM34 modulates influenza virus-activated programmed cell death by targeting Z-DNA-binding protein 1 for K63-linked polyubiquitination. The Journal of Biological Chemistry. 2022; 298: 101611. https://doi.org/10.1016/j.jbc.2022.101611.

[21] Shah H, Hacker A, Langburt D, Dewar M, McFadden MJ, Zhang H, *et al*. Myocardial Infarction Induces Cardiac Fibroblast Transformation within Injured and Noninjured Regions of the Mouse Heart. Journal of Proteome Research. 2021; 20: 2867–2881. https://doi.org/10.1021/acs.jproteome.1c00098.

[22] Daseke MJ, 2nd, Tenkorang MAA, Chalise U, Konfrst SR, Lindsey ML. Cardiac fibroblast activation during myocardial infarction wound healing: Fibroblast polarization after MI. Matrix Biology: Journal of the International Society for Matrix Biology. 2020; 91-92: 109–116. https://doi.org/10.1016/j.matbio.2020.03.010.

[23] Lian Q, Yan S, Yin Q, Yan C, Zheng W, Gu W, *et al*. TRIM34 attenuates colon inflammation and tumorigenesis by sustaining barrier integrity. Cellular & Molecular Immunology. 2021; 18: 350–362. https://doi.org/10.1038/s41423-020-0366-2.

[24] Ying H, Guo W, Yu P, Qiu H, Jiang R, Jiang C. Characteristics of immune clusters and cell abundance in patients with different subtypes of nonparoxysmal atrial fibrillation. Scientific Reports. 2023; 13: 968. https://doi.org/10.1038/s41598-022-26749-z.

[25] Yoon H, Tang CM, Banerjee S, Delgado AL, Yebra M, Davis J, *et al*. TGF-β1-mediated transition of resident fibroblasts to cancer-associated fibroblasts promotes cancer metastasis in gastrointestinal stromal tumor. Oncogenesis. 2021; 10: 13. https://doi.org/10.1038/s41389-021-00302-5.

[26] Tan S, Spear R, Zhao J, Sun X, Wang P. Comprehensive Characterization of a Novel E3-Related Gene Signature With Implications in Prognosis and Immunotherapy of Low-Grade Gliomas. Frontiers in Genetics. 2022; 13: 905047. https://doi.org/10.3389/fgene.2022.905047.

[27] Bilbao D, Valcárcel J. Getting to the heart of a splicing enhancer. Nature Structural Biology. 2003; 10: 6–7. https://doi.org/10.1038/nsb0103-6.

[28] Zhang H, Kou X, Xiao D, Yu Z. Long non-coding RNA lincRNA-erythroid prosurvival attenuates inflammation by enhancing myosin heavy chain 6 stability through recruitment of heterogeneous nuclear ribonucleoprotein L in myocardial infarction. Bioengineered. 2022; 13: 14426–14437. https://doi.org/10.1080/21655979.2022.2086376.

[29] Ikushima H, Miyazono K. TGFbeta signalling: a complex web in cancer progression. Nature Reviews. Cancer. 2010; 10: 415–424. https://doi.org/10.1038/nrc2853.

[30] Wu Y, Luo J, Song X, Gu W, Wang S, Hao S, *et al*. Irisin attenuates angiotensin II-induced atrial fibrillation and atrial fibrosis via LOXL2 and TGFβ1/Smad2/3 signaling pathways. Iranian Journal of Basic Medical Sciences. 2023; 26: 717–724. https://doi.org/10.22038/IJBMS.2023.68639.14967.

[31] Xiao Y, Ni L, Shi H, Yang K, Yang J, Zhao J, *et al*. SAA1 deficiency alleviates cardiac remodeling by inhibiting NF-

κB/p38/JNK and TGFβ/Smad pathways. FASEB Journal: Official Publication of the Federation of American Societies for Experimental Biology. 2023; 37: e22911. https://doi.org/10.1096/fj.202201506R.

[32] Sharma M, Singh TU, Rana A, Kumar T, Gari M, Mani P, *et al*. Biochanin-A alleviates fibrosis and inflammation in cardiac injury in mice. Journal of Biochemical and Molecular Toxicology. 2023; 37: e23360. https://doi.org/10.1002/jbt.23360.

[33] Yu J, Zhao X, Yan X, Li W, Liu Y, Wang J, *et al*. Aloe-emodin ameliorated MI-induced cardiac remodeling in mice via inhibiting TGF-β/SMAD signaling via up-regulating SMAD7. Phytomedicine: International Journal of Phytotherapy and Phytopharmacology. 2023; 114: 154793. https://doi.org/10.1016/j.phymed.2023.154793.

[34] Song X, Nie L, Long J, Zhao J, Liu X, Wang L, *et al*. Hydrogen sulfide alleviates hypothyroidism-induced myocardial fibrosis in rats through stimulating autophagy and inhibiting TGF-β1/Smad2 pathway. The Korean Journal of Physiology & Pharmacology: Official Journal of the Korean Physiological Society and the Korean Society of Pharmacology. 2023; 27: 1–8. https://doi.org/10.4196/kjpp.2023.27.1.1.

[35] Ren LL, Li XJ, Duan TT, Li ZH, Yang JZ, Zhang YM, *et al*. Transforming growth factor-β signaling: From tissue fibrosis to therapeutic opportunities. Chemico-biological Interactions. 2023; 369: 110289. https://doi.org/10.1016/j.cbi.2022.110289.